Available online at www.sciencedirect.com
SCIENCE DIRECT®
ELSEVIER
International Journal of Plasticity 20 (2004) 2233–2248
INTERNATIONAL JOURNAL OF Plasticity
www.elsevier.com/locate/ijplas

Quasi-static and dynamic loading responses and constitutive modeling of titanium alloys

Akhtar S. Khan *, Yeong Sung Suh [1], Rehan Kazmi

Department of Mechanical Engineering, University of Maryland, Baltimore County, Baltimore, MD 21250, USA

Received in final revised form 16 June 2003
Available online 17 July 2004

Abstract

The results from a systematic study of the response of a Ti–6Al–4V alloy under quasi-static and dynamic loading, at different strain rates and temperatures, are presented. The correlations and predictions using modified Khan–Huang–Liang (KHL) viscoplastic constitutive model are compared with those from Johnson–Cook (JC) model and experimental observations for this strain rate and temperature-dependent material. Overall, KHL model correlations and predictions are shown to be much closer to the observed responses, than the corresponding JC model predictions and correlations. Similar trend has been demonstrated for other titanium alloys using published experimental data [Mech. Mater. 33(8) (2001) 425; J. Mech. Phys. Solids 47(5) (1999) 1157].

Keywords: Constitutive behavior; Elastic–viscoplastic material; Finite dynamic strain; Titanium alloy; Split Hopkinson bar; Thermal softening; High strain-rate response; Kolsky bar

1. Introduction

Dynamic deformation has been of interest not only in impact and penetration related problems (Gilat and Cheng, 2002; Khan et al., 2002; Khan and Lopez-Pa-

* Corresponding author. Tel.: +1-410-455-3301; fax: +1-410-455-1052.
E-mail addresses: khan@umbc.edu (A.S. Khan), suhy@hannam.ac.kr (Y. Sung Suh).
[1] On leave from Department of Mechanical Engineering, Hannam University, Daejeon 306-791, Republic of Korea.

0749-6419/$ - see front matter © 2004 Published by Elsevier Ltd.
doi:10.1016/j.ijplas.2003.06.005

mies, 2002; Bjerke et al., 2002) but also in high speed machining (Molinari et al., 2002; Burns and Davies, 2002); titanium alloys have been studied by several investigators because of their use in aero-engine, gas turbines and other applications due to their high strength to weight ratio, ductility, and ability to withstand high temperatures and resist corrosion. Examples are Macdougall and Harding (1999), Meyers et al. (1994), Chichili et al. (1998), Cheng and Nemat-Nasser (2000). The first investigation mentioned above was on Ti–6Al–4V alloy, while others were on commercially available pure α-titanium except in case of Cheng and Nemat-Nasser (2000), in which the microstructure, typer or phase, was not specified. The development of relatively economical Ti–6Al–4V alloy, with resulting high oxygen content, has sparked interest in its possible use in lightweight tanks (Montgomery and Wells, 2001); the conventional, more expensive Ti–6Al–4V alloy has been used primarily in aerospace components. The potential applications in armor, including ceramic tiles encapsulated in titanium alloys, have motivated several studies (Gray III, 1997; Follansbee and Gray, 1989; Lesuer, 2000; Nemat-Nasser et al., 2001; Majorell et al., 2002).

In case of α-titanium, it has been demonstrated that the deformation mechanisms include glide systems with a-type dislocations in the hcp structure, as well as, twinning shear which contributed to the overall strain (Meyers et al., 1994; Song and Gray III, 1995; Chichili et al., 1998). In the only quantitative study of twinning, Chichili et al. (1998) have shown that twin number density increases drastically with increase in strain rate. They used length-to-diameter ratio of 1.6 for quasi-static experiments. The rate of increase of this density decreased with increase in strain at dynamic strain-rates of 10^3 s^{-1}, while this rate increased with deformation in the case of quasi-static loading (10^{-5} s^{-1}). Their results further demonstrated that loading at a particular temperature (and/or strain rate), unloading, and reloading at another temperature (and/or strain rate), resulted in a stress–strain curve which was significantly different than if the specimen was loaded at the latter temperature (and/or strain rate) right from the beginning. This study was performed over a wide range of strain rates (10^{-3}–10^3 s^{-1}) but over a very limited range of temperatures (77–298 K). Further, they did not provide the geometry of the specimens used in their split Hopkinson bar measurements.

The Ti–6Al–4V alloy consists of hcp α-grains, with a dispersion of stabilized bcc β phase around grain boundaries at room temperature. α phase transforms to β phase starting at 873 K (1110 F); above 1268 K (1825 F), the entire microstructure consists of equiaxed β grains (Majorell et al., 2002). This alloy, in addition to H, V, and Ti, contains O, Fe, Mo, C, Si, and Mn. Oxygen, nitrogen, and carbon contents are α stabilizers (Conrad et al., 1973), while vanadium, iron and molybdenum are β stabilizers. Conrad et al. (1973) proposed an equivalent oxygen content ($O_{eq} = O + 2N + 0.75C$); this equivalent impurity concentration gives the effect of dislocations–impurity interaction on the yield strength of the material. Investigation by Majorell et al. (2002) was on an untextured and a textured Ti–6Al–4V alloy rod that was manufactured by Allvac. This study was over a strain-rate range from 10^{-3} to 10 s^{-1} and a temperature range of 650–1345 K (710–1970 F). They did not observe any dynamic strain-aging at any of the temperatures or strain rates investigated.

Further, athermal stress, i.e., temperature insensitive response, was found at approximately 1255 K (1800 F); i.e. at a temperature when the material contained almost 100% β phase. They did not specify specimen geometries used in their investigation. The equivalent oxygen content was 0.206%.

In a study by Follansbee and Gray (1989), on a Ti–6Al–4V alloy, with an equivalent oxygen content of 0.23% (actual oxygen was 0.18%), the measurements were restricted to three temperatures with a range between 76 and 295 K and at only two strain rates (10^{-3} and $\approx 3000\ s^{-1}$). Their specimens on as-received and two heat-treated versions were made from a 13.8 mm thick plate; specimens were 4.8 mm in diameter and 5.2 mm long in case of quasi-static loading experiments, and 6.4 mm diameter with a length of 5.1 mm in a 12.7 mm diameter split Hopkinson bar experiment. This investigation did not include responses over a wide range of temperatures. Nemat-Nasser et al. (2001) study was on a commercial and two hot isostatically pressed Ti–6Al–4V alloys. The equivalent oxygen in the commercially pure alloy was 0.22%. The geometry of the specimens was not specified and was presumably 5 mm in diameter and 5 mm long, for quasi-static and dynamic experiments. The diameters of the split Hopkinson bars (perhaps 12.7 mm) were not specified either in the paper. The measurements and assumptions in this investigation have raised several questions. First, they perform experiments on specimens from 77 to 998 K in the dynamic strain rate regime of 2000–4000 s^{-1}. As discussed earlier, α phase starts transforming to β phase at 873 K. Thus, they performed experiments on presumably different materials in their range of temperatures, i.e., with different amounts of α and β phases. Second, it is clear from Fig. 3(a) in their paper that at least some experiments had barreling due to insufficient lubrication. Third, they combine initial portions of multiple stages loading–unloading–reloading experiments using split Hopkinson bar technique, to obtain "isothermal" response, even when it is well known that initial portion(s) of the stress–strain curve is not accurate as force equilibrium in the specimen is not reached until elastic and plastic waves are reflected several times back and forth in the specimen. Using these loading–unloading and reloading experiments at different temperatures, they suggested that all (i.e. 100%) of plastic work done was converted to heat. This suggestion is in direct contradiction to the measurements of Mason et al. (1994), Liao and Duffy (1998), Macdougall and Harding (1999) and Rosakis et al. (2000). As mentioned earlier, Chichili et al. (1998) and Follansbee and Gray (1989) have shown that the response of a material is different upon reloading to a different temperature (same strain rate), presumably due to history effects.

Similar inadequacies and contradictions are found in the published modeling efforts. The constitutive models used for high strain rate applications can be classified in two categories; the purely phenomenological ones, e.g., Johnson–Cook (JC) (Johnson and Cook, 1983) and Khan–Huang–Liang (KHL) models (Khan and Huang, 1992; Khan and Liang, 1999; Khan and Zhang, 2000, 2001) and so-called, "physically based models" e.g., the ones by Zerilli and Armstrong (1987), Mecking and Kocks (1981), etc., that were used frequently by Follansbee and Gray (1989), and in a modified form by Nemat-Nasser et al. (2001). The latter group discusses the mechanisms of plastic deformation, mainly dislocations. However, the material

constants are determined by not measuring any deformation mechanism related quantity, but by choosing constants to "fit" the uniaxial stress–strain curves at different strain rates and temperatures, just like the purely phenomenological models. In order to "fit" their model to the uniaxial stress–strain curves of two fairly close Ti–6Al–4V alloys, Nemat-Nasser et al. (2001) used athermal stress of 685 MPa while Follansbee and Gray (1989) used 100 MPa; Follansbee and Gray (1989) used a value of 10 MPa to analyze results of Paton et al. It is disappointing to note that there is almost 600% difference in this value by these two set of researchers using models that are presumably based on the same "physics" for very similar materials. In the original Mecking and Kocks model, as used by Follansbee and Gray (1989), a highly undesirable extrapolation to 0 K is necessary. In addition, the model has numerous material constants; it requires huge amount of resources and time to determine these constants. In the simplification or modification of this model by Nemat-Nasser et al. (2001), experiments are needed at very high temperatures where proper lubrication is extremely difficult, if not impossible, to attain, as is clearly evident in their Fig. 3(a) of their paper. Since both categories of models, phenomenological and "so-called physically based", determine material constants by "fitting" to the stress–strain responses at different temperatures and strain rates, the advantage of one over the other is merely number of material constants in each model. Any model with semi-infinite number of material constants will be able to approximate observed responses. Mecking and Kocks model, as used by Follansbee and Gray (1989) has 23 constants, while these constants range from 12 to 8 in case of Cheng and Nemat-Nasser (2000) and Nemat-Nasser et al. (2001), respectively, depending on whether they include modeling of dynamic strain aging or not. Johnson–Cook and Khan–Huang–Liang models have 5 and 6 constants, respectively. Johnson–Cook and Khan–Huang–Liang models are used in this investigation due to their advantage of fewer constants and their ability to model the observed material response as closely as with models with many more constants.

2. Modeling approach

The material constants for both, the modified KHL and JC models were determined. Using these material constants, correlations were obtained and compared to experimental results. The modified KHL model is as follows:

$$\sigma = \left[A + B\left(1 - \frac{\ln \dot{\varepsilon}}{\ln D_0^{\mathrm{p}}}\right)^{n_1} (\varepsilon^{\mathrm{p}})^{n_0}\right]\left(\frac{\dot{\varepsilon}}{\dot{\varepsilon}^*}\right)^{C}\left(\frac{T_{\mathrm{m}} - T}{T_{\mathrm{m}} - T_{\mathrm{r}}}\right)^{m}, \tag{1}$$

where σ is the stress and ε^{p} is the plastic strain. T_{m}, T, T_{r} are melting, current, and reference temperatures, respectively. $D_0^{\mathrm{p}} = 10^6\ \mathrm{s}^{-1}$ (arbitrarily chosen upper bound strain rate) and $\dot{\varepsilon}^* = 1\ \mathrm{s}^{-1}$ (reference strain rate at which some material constants are determined). $\dot{\varepsilon}$ is the current strain rate. A, B, n_1, n_0, C and m are material constants. For Ti–6Al–4V alloys, the melting temperature is 1933 K (Nemat-Nasser et al., 2001). A major feature of this model, unlike the JC model, is that decreasing work-

hardening with increasing strain rate can be accommodated through the material constant n_1. Previously, this model had a temperature dependence term (similar to JC model) as

$$\left(1-\left(\frac{T-T_{\mathrm{r}}}{T_{\mathrm{m}}-T_{\mathrm{r}}}\right)^{m}\right). \tag{2}$$

However, this term cannot accommodate the case when the current temperature is lower than the reference temperature as then the above term within parenthesis becomes a negative number raised to the power m. Therefore a modification was made as given in Eq. (1). The JC model is given by the following equation:

$$\sigma=[A+B(\varepsilon^{\mathrm{p}})^{n_0}]\left(1+C\ln\frac{\dot{\varepsilon}}{\dot{\varepsilon}^{*}}\right)\left(1-\left(\frac{T-T_{\mathrm{r}}}{T_{\mathrm{m}}-T_{\mathrm{r}}}\right)^{m}\right). \tag{3}$$

In this case, various terms have the same definitions as Eq. (1).

To determine the material constants for the model, uniaxial loading test results at different strain rates and temperatures were first used to obtain an initial set of values for the material constants, as described in Khan and Liang (1999). In order to get a refined set of material constants, the least-squares and a constrained optimization procedures were used to minimize the difference between correlated and actual data using MATLAB. The experimental results at low strain rates were first used to get a set of material constants using the least-squares method. Then, higher strain rate data, measured under adiabatic condition, were correlated with the assumption that 90% plastic work was dissipated to heat, to get a better set of material constants for both low and high strain rate material response using a constrained optimization procedure. This was iteratively performed until the constants converged. As for the dynamic data, thermal softening from the adiabatic deformation was effectively considered by converting the increment of temperature from the stress–strain curve using following equation:

$$\Delta T=\frac{\beta}{\rho C_{\mathrm{p}}}\int_{0}^{\varepsilon_1^{\mathrm{p}}}\sigma(\varepsilon^{\mathrm{p}})\,\mathrm{d}\varepsilon^{\mathrm{p}}, \tag{4}$$

where β, ρ, C_{p} are the fraction of heat dissipation caused by the plastic deformation, mass density and specific heat at constant pressure, respectively. In fact, there are many arguments on the conversion of plastic work to heat during high strain rate deformation. Taylor and Quinney (1934) measured the fraction of heat conversion and found that it is of the order of 0.9 with copper specimens. Mason et al. (1994) measured it with dynamic experiments and demonstrated that it depended substantially on strain and strain rate. Kapoor and Nemat-Nasser (1998) measured the energy converted to heat using an infra-red method for Ta–2.5% W alloy, commercially pure Ti, 1018 steel, 6061 Al and OFHC Cu. They argued that the infra-red measurement generally underestimated the conversion ratio (70% of conversion of work for Ta–2.5% W, for example), they cooled down the specimen to the initial room temperature at certain strain and heated it to the temperature based on 100% heat conversion and then deformed the specimen at the same strain

rate to check if the adiabatic curve was obtained. On this basis, they suggested that nearly all of the plastic work was converted into heat (i.e., $\beta = 1$) within experimental error, concluding that the infra-red detection system recorded a lower (surface) temperature than the actual temperature of the specimen. Later, Nemat-Nasser et al. (2001) argued for this total heat conversion by measuring the thermomechanical response of a Ti–6Al–4V alloy (commercial Ti64). Macdougall and Harding (1999) calculated the proportion of work converted to heat based on their torsional dynamic test with an infrared technique for Ti–6Al–4V specimens and concluded that β varied with increasing plastic strain from approximately 0.2 to approaching 0.7. Rittel (1999) and Rosakis et al. (2000) also indicated that β was a history-dependent quantity and depended strongly on both strain and strain rate for various engineering materials. There seems to be no agreement on a single value of β that works for variety of engineering materials, however, most researchers still use 0.9, e.g., Lennon and Ramesh (2004). In this study, $\beta = 0.9$ was assumed.

For Ti–6Al–4V, the density is $\rho = 4428$ kg/m^3 (Lesuer, 2000). The heat capacity was expressed as a function of the temperature (Military Handbook, 1998)

$$C_p = 559.77 - 0.1473T + 0.00042949T^2 \text{ J/(kg K)} \quad (278 \text{ K} < T < 1144 \text{ K}). \tag{5}$$

Finally, using these material constants for both models, predictions were made and compared to a strain-rate-jump experiment (from 10^{-5} to 10^{-1} to 1700 s^{-1}).

Material constants for both models were determined for two additional Ti–6Al–4V alloys (Nemat-Nasser et al., 2001; Macdougall and Harding, 1999). The first one was commercially available from Protech Metals (Nemat-Nasser et al., 2001), and the second one was used in torsion and tension tests by Macdougall and Harding (1999), where the exact composition of the Ti–6Al–4V was not given.

3. Experimental details

3.1. Material

The chemical composition of Ti–6Al–4V is shown in Table 1. This Ti–6Al–4V alloy is ductile and has a hexagonal close packed crystalline structure. The composition is slightly differed from the commercial Ti alloy that was used by Nemat-Nasser et al. (2001), and is presented in Table 2.

Table 1
Chemical composition of Ti–6Al–4V (Alloy 1) in the present investigation

Element	Ti	Y	N	C	H	Fe	O	Al	V
Percent weight composition	Bal.	<0.0003	0.008	0.043	0.0041	0.15	0.174	5.97	4.09

Table 2
Chemical composition of commercial Ti–6Al–4V (Alloy 2) used by Nemat-Nasser et al. (2001)

Element	Ti	Y	N	C	H	Fe	O	Al	V
Percent weight composition	Bal.	<0.001	0.01	0.01	0.0006	0.21	0.19	6.21	3.61

3.2. Experimental procedure

3.2.1. Room temperature compression experiments

Quasi-static compression experiments were conducted using an MTS servo hydraulic axial/torsional material testing machine at strain rates from 10^{-5} to 1 s^{-1}, using cylindrical specimens. The specimens were machined from a plate (27.9 mm thick) of Ti–6Al–4V to 19.1 mm in length and 12.7 mm in diameter. The length dimension was in the thickness direction of the plate. It should be noted that the experiment at a strain rate of 1 s^{-1} was conducted in increments of 5% strain, with 30 min between loading and reloading. This method allowed the specimen sufficient time to cool, ensuring an isothermal response. For room temperature compression experiments, KFEL-2-120-C1 high elongation uniaxial strain gages, manufactured by Kyowa Ltd. (Japan), were mounted diametrically opposite to each other at the center of each specimen using Micro-Measurements Inc. adhesive AE-15. The MTS transducers directly supplied load and LVDT output data to the TestStar software. The interface between the load platens and the test specimens for each of the compression experiments was lubricated with Teflon sheets and Dow Corning high vacuum grease in order to achieve homogeneous deformation and thus avoid barreling of the specimen, maintaining a uniform, uniaxial stress state.

3.2.2. Compression experiments at different temperatures

Quasi-static experiments at different temperature were conducted at 233, 296, 422, 588, and 755 K with a strain rate of 10^{-3} s^{-1}. The LVDT displacement supplied stroke data that included the total deformation of the MTS actuators, the loading platens, the grease lubricant, and the specimen. The interface between the load platens and the test specimens for each of the compression experiments was lubricated with high or low temperature grease, depending on the experiment temperature, in order to achieve uniformity in deformation and avoid barreling of the specimen, maintaining a uniform, uniaxial stress state. The stroke was corrected by running a blank experiment (without specimen).

3.2.3. Dynamic compression experiments

The split Hopkinson bar technique was used to attain a dynamic measurements. The interfaces between the incident and transmitted bars and the test specimen were carefully lubricated with grease, in order to increase uniformity in deformation. The initial thickness and diameter of the specimen were 5.1 (in the direction of thickness of the plate) and 10.2 mm, respectively. The pressure and striker bars used for the experiment were made of hardened VascoMax C350 steel and the diameters were 12.7 mm.

3.2.4. Room temperature strain-rate-jump-compression experiments

In order to conduct the strain-rate-jump experiment, the specimen was loaded at an initial strain rate of 10^{-5} s^{-1}. The strain rate was then increased to 10^{-1} s^{-1} around 6.3% strain. Upon unloading the specimen after quasi-static compression, around 14% strain, it was machined into two dynamic compression specimens with diameter 10.2 mm and thickness 5.1 mm. The split Hopkinson pressure bar technique was then used to obtain the response of the material in the third stage of loading at a strain rate of 1700 s^{-1}.

4. Results and discussion

4.1. Experimental results

Fig. 1 includes the measured true stress–true plastic strain curves shown with symbols (the plastic strain was converted from the total strain measurement) at different strain rates and at room temperature. As seen in Fig. 1, the material response at various strain rates indicates that the material is strain rate dependent. Fig. 2 gives the measured true stress–true plastic strain curves (also shown with

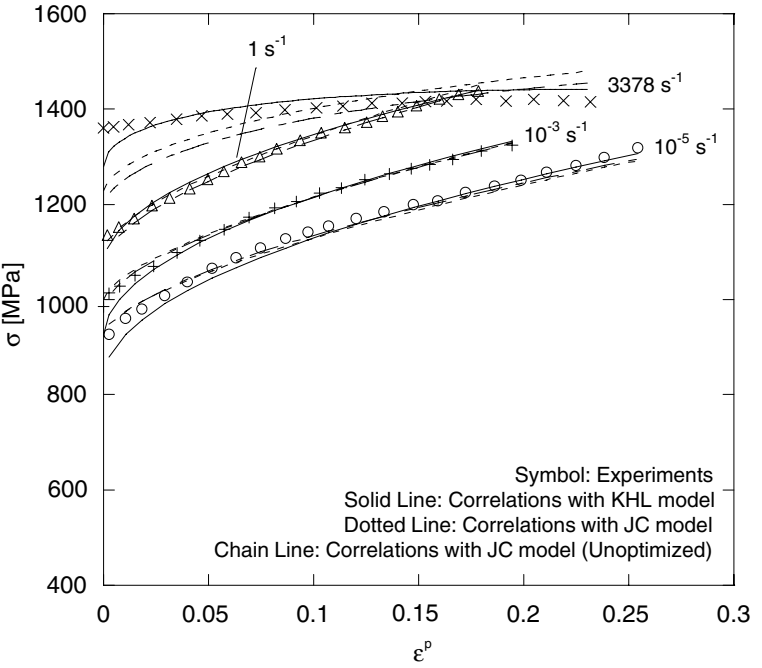

Fig. 1. Quasi-static and dynamic loading experimental results (at a temperature of 296 K) for different strain rates with correlations using KHL and JC models; the correlations with JC model were shown with and without optimization to determine the material constants.

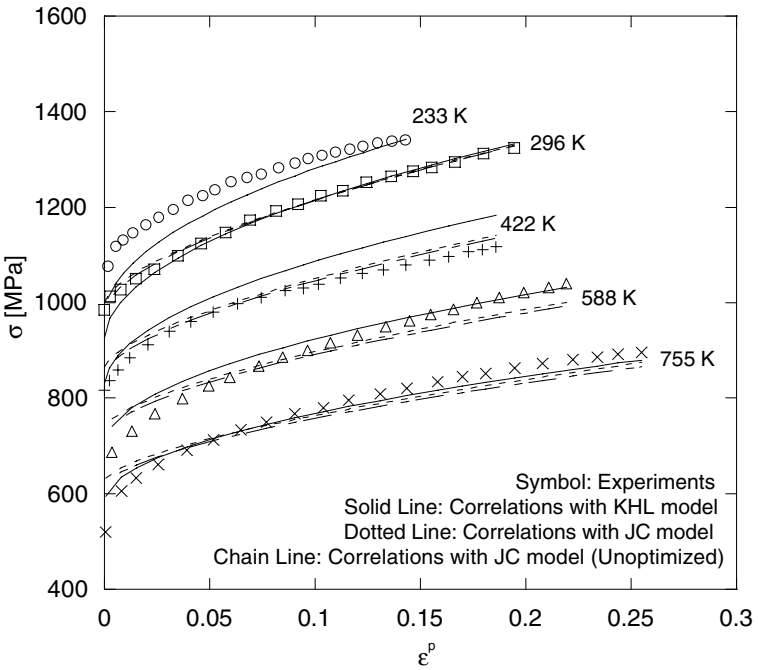

Fig. 2. Quasi-static measurements (at a strain rate of 10^{-3} s^{-1}) for various temperatures with correlations using KHL and JC models; the correlations with JC model were shown with and without optimization to determine the material constants. Note the absence of correlation at 233 K with JC model in which $(T - T_{ref})/(T_m - T_{ref})$ becomes negative.

symbols) at different temperatures and at a strain rate of 10^{-3} s^{-1}. Figs. 1–3 include results using the Alloy 1 (see Table 1). Fig. 4 contains results of Nemat-Nasser et al. for Alloy 2, while Figs. 5 and 6 represent results of Macdougall and Harding (1999).

4.2. Determination of material constants

In order to determine the material constants, all data were included in the least-squares method and constrained optimization procedure. Isothermal dynamic response was obtained, and included in the optimization procedure, from adiabatic measurements using $\beta = 0.9$. In case of JC model, the material constants were determined by two methods, the published non-optimized approach and also the optimized method used for KHL method. Tables 3 and 4 include material constants for KHL and JC models, determined for Ti–6Al–4V alloy and for two alloys from the studies of the data extracted from Nemat-Nasser et al. (2001) and Macdougall and Harding (1999).

4.2.1. Correlations and predictions with Ti–6Al–4V (Alloy 1)

The quasi-static and dynamic measurements at a temperature of 296 K and at various strain rates, along with correlations by KHL and JC models are shown in

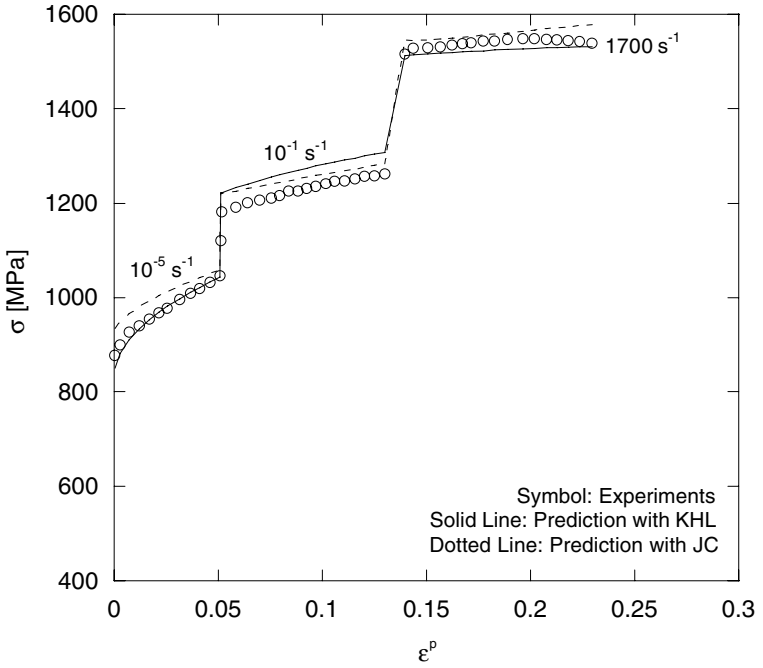

Fig. 3. A comparison of a strain-rate-jump experiment results with predictions using KHL and JC models. The test was performed at 296 K with strain rate from 10^{-5} to 10^{-1} s^{-1} and to 1700 s^{-1}. The predictions were made assuming that 10^{-5} s^{-1} region is under isothermal conditions, while 10^{-1} and 2800 s^{-1} regions are under adiabatic condition. Material constants for JC model used here were determined with optimization.

Fig. 1. Although the correlations with both models are reasonably good for the quasi-static case, the KHL model correlates better with the dynamic response, while the JC model differs substantially from the measured response in terms of initial yield stress and work hardening rate at this high strain rate deformation. It was observed that even with the optimized material constants, JC model did not correlate well with the dynamic response. This is due to the fact that JC model fails to correlate the decreasing work hardening rate as the strain rate increases. This is described elsewhere in detail (Liang and Khan, 1999), in which it was shown that in the JC model, the work hardening rate at certain strain would increase when strain rate increases. That is, the JC model is not appropriate for modeling any material where the work hardening rate decreases with increasing strain rate, such as tantalum (Chen and Gray, 1995). With Ti–6Al–4V, too, it can be observed from the material behavior at different strain rates that the work hardening rate decreases as the strain rates increases.

In Fig. 2, quasi-static measurements (at a strain rate of 10^{-3} s^{-1}) at various temperatures, with correlations using KHL and JC models are shown, respectively. Material constants for JC model determined using published conventional methods,

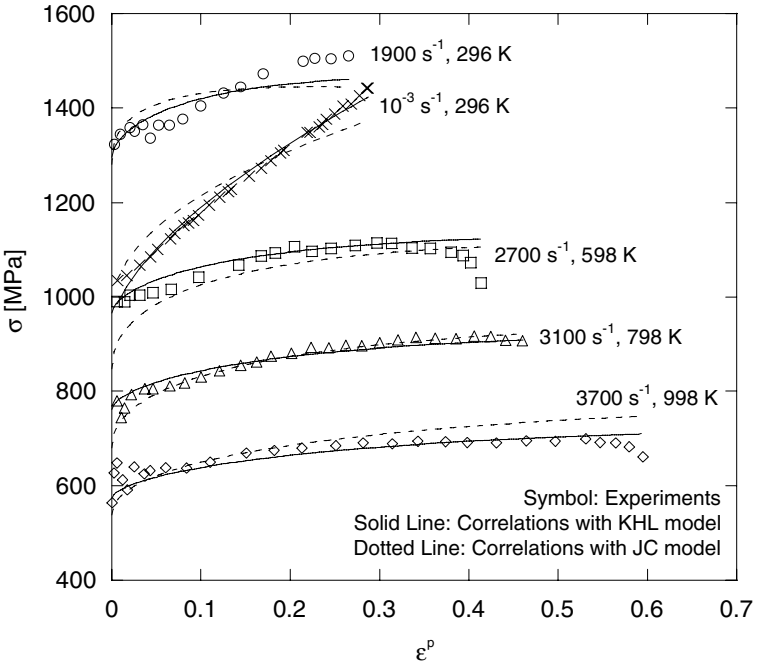

Fig. 4. Quasi-static (at a strain rate of 10^{-3} s^{-1}) and dynamic measurements for various strain rates and temperatures (Nemat-Nasser et al., 2001) with correlations using KHL and JC models. Material constants for JC model used here were determined with optimization.

i.e., without the optimization, led to slight deviation from the measured response. Overall, the KHL model gave somewhat better correlation than the JC model, except for 422 K. The JC model has a major drawback that it cannot be used at temperatures lower than the reference temperature at which material constants are determined. Note the absence of correlation at 233 K in JC model as, $(T - T_{\text{ref}})/(T_{\text{m}} - T_{\text{ref}})$ becomes negative.

A strain-rate-jump experiment was performed at 296 K with strain rate from 10^{-5} to 10^{-1} s^{-1}, followed by an experiment at a strain rate of 1700 s^{-1}. The measured response was compared with predicted ones by using KHL and JC models (Fig. 3). This experimental response was not included in the determination of material constants. The predictions were made assuming that 10^{-5} s^{-1} span is under isothermal conditions and 10^{-1} and 1700 s^{-1} experiment are under adiabatic condition. Especially at a strain rate of 1700 s^{-1}, and initial segment at 10^{-5} s^{-1}, KHL model predictions are in better agreement with the measured responsethan the JC model, which overpredicts the experimental results at these two strain rates.

4.2.2. Correlations with Nemat-Nasser et al.'s data (Alloy 2)

In Fig. 4, quasi-static and dynamic measurements (at a strain rate of 10^{-3} s^{-1}) for various temperatures with the correlations using KHL and JC models are shown.

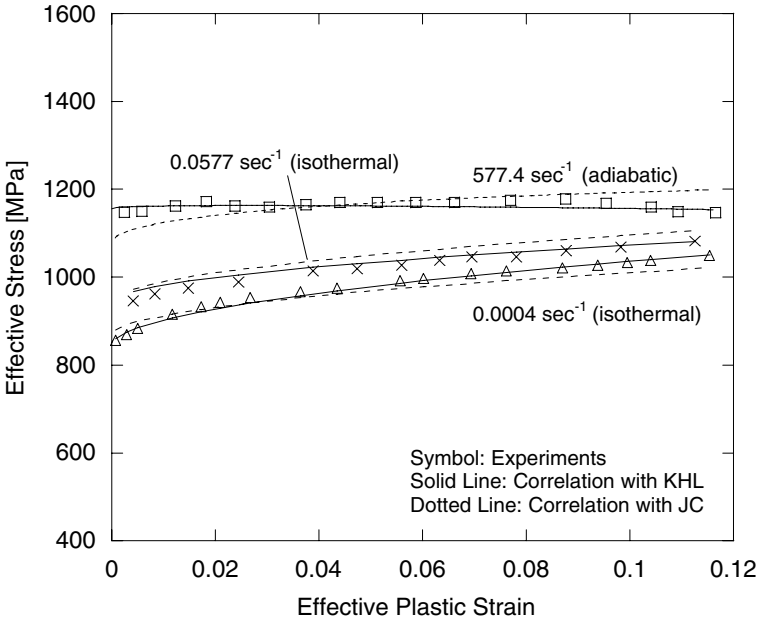

Fig. 5. Quasi-static and dynamic torsional measurements for effective strain rates, $\dot{\bar{\varepsilon}} = 577.4$, 0.0577, and 0.0004 s^{-1} at a temperature of 293 K (Macdougall and Harding, 1999) with correlations using KHL and JC models. Material constants for JC model used here were determined with optimization.

These measurements were made on a commercially available Ti–6Al–4V alloy, obtained from Protech Metals. As shown in Table 2, the composition of this material is somewhat different from that of the Ti–6Al–4V alloy studied in the present work (Alloy 1), see Table 1. Since the quasi-static data to determine the initial material constants were not available, the parameters were directly optimized using the parameters obtained for the other alloy as an initial input. For all the cases, KHL model gives better correlation.

4.2.3. Correlations and predictions using Macdougall and Harding's data (Alloy 3)

The data from torsional experiments were extracted and converted to von Mises effective stress and effective plastic strain assuming $\bar{\sigma} = \tau\sqrt{3}$ and $\bar{\varepsilon}^{p} = \gamma/\sqrt{3}$ where τ and γ are shear stress and shear strain, respectively. The material constants determined from the correlation with three torsional measurements: $\dot{\gamma} = 1000$, 0.1, and 0.0007 s^{-1} (which correspond to effective von Mises strain rates, $\dot{\bar{\varepsilon}} = 577.4$, 0.0577, and 0.0004 s^{-1}, respectively). These constants are given in Tables 3 and 4. Since the data near failure may be affected by necking (tensile loading), or buckling in case of torsional loading, these data near failure are not included in the analysis. In Fig. 5, quasi-static and dynamic torsional measurements with effective strain rates, $\dot{\bar{\varepsilon}} = 577.4$, 0.0577, and 0.0004 s^{-1} at a temperature of 293 K are shown along with correlations using KHL and JC models. The material constants were determined

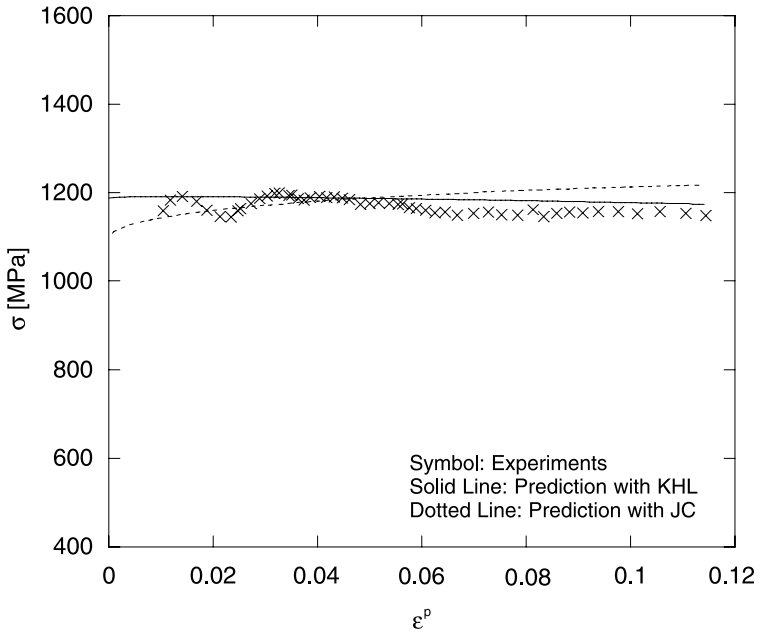

Fig. 6. Comparison between tensile dynamic data with a strain rate, $\dot{\varepsilon} = 2000\ s^{-1}$, and predicted adiabatic responses using KHL and JC models at a temperature of 293 K. The material constants were optimally determined from the correlation with torsional experiments as shown in Fig. 5.

Table 3
KHL model material constants determined for Ti–6Al–4V (Alloy 1) and the data extracted from Nemat-Nasser et al. (2001), Alloy 2, and Macdougall and Harding (1999), Alloy 3

	A (MPa)	B (MPa)	n_1	n_0	C	m
Ti–6Al–4V (Alloy 1)	1069	874.8	0.5456	0.4987	0.02204	1.3916
Ti–6Al–4V (Alloy 2)	1097	1004.7	0.4993	0.6268	0.02219	1.4796
Ti–6Al–4V (Alloy 3)	1004	325.1	1.9015	0.5263	0.02204	1.1206

Table 4
JC model material constants determined for Ti–6Al–4V (Alloy 1) and the data extracted from Nemat-Nasser et al. (2001), Alloy 2, and Macdougall and Harding (1999), Alloy 3

	A (MPa)	B (MPa)	n_0	C	m
Ti–6Al–4V (Alloy 1)					
With optimization	1104	1036	0.6349	0.01390	0.7794
Without optimization	1080	1007	0.5975	0.01304	0.7701
Ti–6Al–4V (Alloy 2)	1119	838.6	0.4734	0.01921	0.6437
Ti–6Al–4V (Alloy 3)	984.0	520.3	0.5102	0.01500	0.8242

from the same experimental results. Again, KHL model correlations are better than those with JC model especially at higher strain rates. Based on the material constants determined only from the torsion experiments, a comparison between tensile

dynamic data at a strain rate, $\dot{\varepsilon} = 2000\ s^{-1}$, and predicted adiabatic stress/strain responses using KHL and JC models at a temperature of 293 K are shown in Fig. 6. Again, KHL model gives better prediction, especially the thermally softened work-hardening due to heat dissipation is more closely predicted with KHL model.

5. Conclusions

A comprehensive study on quasi-static and dynamic responses of a Ti–6Al–4V titanium (Alloy 1) from monotonous and strain-rate-jump compression experiments was performed. Quasi-static experiments, using MTS machine, at room temperature were conducted on cylindrical titanium specimens at strain rates of 10^{-5}, 10^{-3} and 1 s^{-1}, and at temperatures of 233, 296, 422, 588, and 755 K at a strain rate of $10^{-3}\ s^{-1}$. Dynamic response was measured using the split Hopkinson pressure bar (SHPB) technique at strain rates of 3378 s^{-1} at room temperature. Experimental results from uniaxial loading experiments were used to determine material constants for the KHL and JC constitutive models for this titanium alloy. It was found that Ti–6Al–4V is non-linearly dependent on strain rate, as well as temperature.

The KHL model was found to correlate better than JC model especially during dynamic deformation regime. The thermal softening at high strain rates, together with reduction in the work hardening rate with increase in strain rate and strain, was captured much better by the KHL model than the JC model. The temperature term of the modified KHL viscoplastic constitutive model was able to correlate well with the response at a temperature (233 K) which was lower than the reference temperature (296 K); the JC model was not valid in this case.

Material constants of the KHL and JC models, determined previously were used for predictions of the observed material response in a strain-rate-jump experiment to examine the validity of the two models. The test was performed at 296 K with strain rate from 10^{-5} to $10^{-1}\ s^{-1}$ and then to 1700 s^{-1}. Again KHL model provided better agreement with the measured response than the JC model.

In addition to this alloy, results from two more titanium alloys were obtained from the existing publications (Nemat-Nasser et al., 2001; Macdougall and Harding, 1999) and compared with correlations and predictions by using KHL and JC models. Once again, the KHL model was closer to the observed response than JC model especially at high strain rates and at different temperatures.

Acknowledgements

The first author is grateful for the funding of this project by the Army Research Office under cooperative agreement DAAD19-01-1-0635, under the direction of Dr. Bruce LaMattina (Solid Mechanics Program). The first author is also thankful to Dr. Douglas Templeton, Team Leader of Emerging Technologies at US Army TARDEC for funding of the project and guidance. Various help and comments of Dr. Raj Rajendran at the Army Research Office is also gratefully acknowledged.

References

Bjerke, T., Li, Z., Lambros, J., 2002. Role of plasticity in heat generation during high rate deformation and fracture of polycarbonates. International Journal of Plasticity 18 (4), 549–567.

Burns, T.J., Davies, M.A., 2002. On repeated adaiabatic shear band formation during high speed machining. International Journal of Plasticity 18 (4), 487–506.

Chen, S.R., Gray III, G.T., 1995. Constitutive behavior of tungsten experiments and modeling. In: Bose, A., Dowding, R.J. (Eds.), Second International Congress on Tungsten and Refractory Metals, McLean, VA, Metal Powder Industries Federation, Princeton, NJ, p. 489.

Cheng, J., Nemat-Nasser, S., 2000. A model for experimentally observed high-strain-rate dynamic strain aging in titanium. Acta Materialla 48 (12), 3131–3144.

Chichili, D.R., Ramesh, K.T., Hemker, K.J., 1998. The high strain rate response of alpha-titanium: experiments, deformation mechanisms and modeling. Acta Meterialia 46 (3), 1025–1043.

Conrad, H.M., Doner, M., de Meester, B., 1973. Critical review deformation and fracture. In: International Conference on Titanium, Proceedings of Titanium Science and Technology. Massachusetts Institute of Technology, Boston, p. 969.

Follansbee, P.S., Gray III, G.T., 1989. An analysis of the low temperature, low and high strain-rate deformation of Ti–6Al–4V. Metallurgical Transactions A 20 (5), 863–874.

Gilat, A., Cheng, C.-S., 2002. Modeling torsional split Hopkinson bar tests at strain rates above 10,000 per sec. International Journal of Plasticity 18 (5–6), 787–799.

Gray III, G.T., 1997. Influence of strain rate and temperature on the structure, property behavior of high purity titanium. Journal of Physics IV France 7 (3), C3-423–C3-429.

Johnson, G.R., Cook, W.H., 1983. A constitutive model and data for metals subjected to large strains, high strain rates and high temperatures. In: Proceedings of the Seventh International Symposium on Ballistic, The Hague, The Netherlands, 1983, p. 541.

Kapoor, R., Nemat-Nasser, S., 1998. Determination of temperature rise during high strain rate deformation. Mechanics of Materials 27 (1), 1–12.

Khan, A.S., Huang, S., 1992. Experimental and theoretical study of mechanical behavior of 1100 aluminum in the strain rate range 10^{-5}–10^{4} s^{-1}. International Journal of Plasticity 8 (4), 397–424.

Khan, A.S., Liang, R., 1999. Behaviors of three BCC metal over a wide range of strain rates and temperatures: experiments and modeling. International Journal of Plasticity 15 (10), 1089–1109.

Khan, A.S., Zhang, H., 2000. Mechanically alloyed nanocrystalline iron and copper mixture: behavior and constitutive modeling over a wide range of strain rates. International Journal of Plasticity 16 (12), 1477–1492.

Khan, A.S., Zhang, H., 2001. Finite deformation of a polymer: experiments and modeling. International Journal of Plasticity 17 (9), 1167–1188.

Khan, A.S., Colak, O.U., Centala, P., 2002. Compressive failure strengths and modes of woven S2-glass reinforced polyester due to quasi-static and dynamic loading. International Journal of Plasticity 18 (10), 1337–1357.

Khan, A.S., Lopez-Pamies, O., 2002. Time and temperature-dependent response and relaxation of a soft polymer. International Journal of Plasticity 18 (10), 1359–1372.

Lennon, A.M., Ramesh, K.T., 2004. The influence of crystal structure on the dynamic behavior of materials at high temperatures. International Journal of Plasticity 20 (2), 269–290.

Lesuer, D.R., 2000. Experimental investigations of material models for Ti–6Al–4V titanium and 2024-T3 aluminum. In: Final Report, DOT/FAA/AR-00/25, US Department of Transportation, Federal Aviation Administration.

Liang, R., Khan, A.S., 1999. A critical review of experimental results and constitutive models for BCC and FCC metals over a wide range of strain rates and temperatures. International Journal of Plasticity 15 (9), 963–980.

Liao, S.-C., Duffy, J., 1998. Adiabatic shear bands in a TI–6Al–4V titanium alloy. Journal of the Mechanics and Physics of Solids 46 (11), 2201–2231.

Macdougall, D.A.S., Harding, J., 1999. A constitutive relation and failure criterion for Ti6Al4V alloy at impact rates of strain. Journal of the Mechanics and Physics of Solids 47 (5), 1157–1185.

Majorell, A., Srivatsa, S., Picu, R.C., 2002. Mechanical behavior of Ti–6Al–4V at high and moderate temperatures – Part I: experimental results. Materials Science and Engineering A 326 (2), 297–305.

Mason, J.J., Rosakis, A.J., Ravichandran, G., 1994. On the strain and strain rate dependence of the fraction of plastic work converted into heat: an experimental study using high speed infrared detectors and the Kolsky bar. Mechanics of Materials 17 (2-3), 135–145.

Mecking, H., Kocks, U.F., 1981. Kinetics of flow and strain-hardening. Acta Metallurgica 29 (11), 1865–1875.

Meyers, M.A., Subhash, G., Kad, B.K., Prasad, L., 1994. Evolution of microstructure and shear-band formation in A-hcp titanium. Mechanics of Materials 17 (2-3), 175–193.

Military Handbook, Metallic Materials and Elements for Aerospace Vehicle Structures, MIL-HDBK-5H, DOD and FAA, 1998.

Molinari, A., Musquar, C., Sutter, G., 2002. Adiabatic shear banding in high speed machining of Ti–6Al–4V: experiments and modeling. International Journal of Plasticity 18 (4), 443–459.

Montgomery, J.S., Wells, M.G.H., 2001. Titanium armor applications in combat vehicles. JOM 53 (4), 29–32.

Nemat-Nasser, S., Guo, Wei-Guo, Nesterenko, Vitali, F., Indrakanti, S.S., Gu, Ya-Bei, 2001. Dynamic response of conventional and hot isostatically pressed Ti–6Al–4V alloys: experiments and modeling. Mechanics of Materials 33 (8), 425–439.

Rittel, D., 1999. On the conversion of plastic work to heat during high strain rate deformation of glassy polymers. Mechanics of Materials 31 (2), 131–139.

Rosakis, P., Rosakis, A.J., Ravichandran, G., Hodowany, J., 2000. A thermodynamic internal variable model for the partition of plastic work into heat and stored energy in metals. Journal of Mechanics and Physics of Solids 48 (3), 581–607.

Song, S.G., Gray III, G.T., 1995. Structural interpretation of the nucleation and growth of deformation twins in Zr and Ti – I. Application of the coincidence site lattice (CSL) theory to twinning problems in H.C.P. structures. Acta Metallurgica et Materialia 43 (6), 2325–2337.

Taylor, G.I., Quinney, H., 1934. The latent energy remaining in a metal after cold working. Proceedings of the Royal Society Series A 143, 307–326.

Zerilli, F.J., Armstrong, R.W., 1987. Dislocation-mechanics-based constitutive relations for material dynamics calculations. Journal of Applied Physics 61 (5), 1816–1825.